

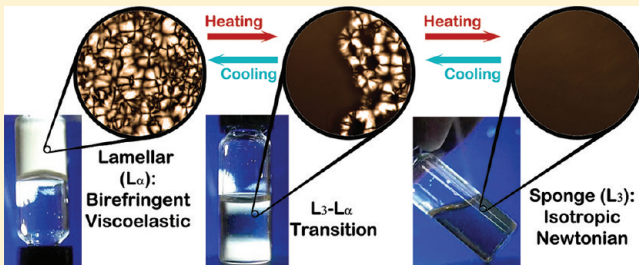
Sponge-to-Lamellar Transition in a Double-Tail Cationic Surfactant/Protic Ionic Liquid System: Structural and Rheological Analysis

Carlos R. López-Barrón, Madivala G. Basavaraj, Leo DeRita, and Norman J. Wagner*

Center for Neutron Science, Department of Chemical Engineering, University of Delaware, Newark, Delaware 19716, United States

W Web-Enhanced

ABSTRACT: The self-assembly of didodecyldimethylammonium bromide (DDAB) in a protic ionic liquid, ethylammonium nitrate (EAN), in the high surfactant concentration regime is studied using five different experimental techniques. A thermoreversible first-order sponge (L_3) to lamellar (L_α) transition occurring at $[DDAB] > 80$ wt % was identified by (1) a sharp increase in the elastic and viscous moduli, (2) a transition peak recorded by differential scanning calorimetry, (3) formation of Maltese cross birefringence textures observed via polarizing optical microscopy, (4) a decrease in the interbilayer mean distance measured by small angle neutron scattering, and (5) an abrupt increase in the conductivity obstruction factor. In contrast to aqueous DDAB solutions, this surfactant forms a stable L_3 phase in EAN in a wide window of compositions and temperatures, which is potentially useful for the synthesis of nanoporous materials. To the best of our knowledge, this is the first evidence of the formation of the L_3 phase in an ionic liquid.



INTRODUCTION

Because of their amphiphilic character, surfactant molecules self-assemble into a large variety of different structures when they are dissolved in a polar solvent (e.g., water). One of these structures is the so-called L_3 phase, which consists of a sponge-like fluid (bilayer) membrane that divides the solvent into bicontinuous phases.^{1,2} This phase is an isotropic liquid with high fluidity³ that displays relatively short-range order.⁴ A number of potential applications include drug delivery carriers,^{5–7} as templates for nanoporous ceramics,^{8–10} and as a model for intracellular membranes.¹¹ The L_3 phase was first reported by Lang and Morgan in the $C_{10}E_4$ /water system,¹² and it has been found in many other amphiphilic systems.^{13–15} However, in aqueous systems, this phase exists only as a metastable state¹⁶ or in narrow regions of stability, adjacent to dilute lamellar (L_α) phases. Accordingly, a stable L_3 phase is highly desirable.

The L_α phase is a stack of parallel layers of thickness δ , with periodicity d . Both the L_α and L_3 phases have the same local structure (i.e., bilayer membranes) but different correlation lengths. Because they are typically adjacent in the surfactant phase diagrams, a change in composition or temperature results in a L_3 – L_α phase transition. This transition is driven by two major energetic factors: One is the variation in the elastic energy driven by the saddle splay rigidity of the bilayer, \overline{K} (i.e., the Gaussian curvature);^{17–20} the second is the entropy-driven order–disorder transition.²¹ For nonionic systems, the L_3 – L_α phase transition can be successfully modeled in terms of the spontaneous curvature and bending moduli.²²

Ionic liquids are salts with poorly coordinated ions, which results in substances having melting temperatures (mp) below

100 °C, or even below room temperature (room temperature ionic liquids, RTILs). Because of their appealing set of properties (including high thermal stability, high ionic conductivity with wide electrochemical windows, and negligible vapor pressure^{23–25}), ILs are well recognized as promising media for reactions^{26–28} and separations.²⁹ A subclass of ionic liquids, protic ionic liquids (PILs), are formed by proton transfer from a Brønsted acid to a Brønsted base. Although the synthesis of the first RTIL, ethylammonium nitrate (EAN, a PIL with mp = 14 °C) dates back to 1914,³⁰ its use as self-assembly media is rather recent.^{31–38}

EAN shares many properties with water, including formation of three-dimensional hydrogen bond structures, which results in the solvophobic effect, which is responsible for micelle formation in both liquids.^{31,39} Of specific interest here is the double-tail cationic surfactant: didodecyldimethylammonium bromide (DDAB), the self-assembly of which has been studied extensively in water because of its industrial relevance.⁴⁰ DDAB has not been previously studied in ionic liquids. However, work on single-tail cationic surfactant/EAN solutions by Evans and co-workers^{31,32} demonstrates that the critical micelle concentration is shifted to a surfactant concentration an order of magnitude higher in comparison to water. In a separate paper, we report the spontaneous thermoreversible formation of stable unilamellar vesicles coexisting with the L_3 phase in DDAB/EAN solutions at low and intermediate concentrations.⁴¹ The stability and spontaneity of formation of both vesicles and the L_3 phase is due to two effects:

Received: June 14, 2011

Revised: September 12, 2011

Published: November 02, 2011

the weak solvophobic strength in EAN and the dynamic ($\text{Br}^- - \text{NO}_3^-$) ion exchange at the palisade layer, which suggest that EAN acts as both solvent and cosurfactant.

Zemb and co-workers reported the phase behavior of DDAB/water solutions.^{16,42–44} At concentrations ranging from 3 to 30 wt %, they observed a swollen lamellar phase (L_α), which shows a linear swelling behavior in the range of 100–700 Å. A collapsed lamellar (L_α') with periodicity of 31 Å exist at concentrations ranging from 75 to 85 wt %. Both lamellar phases have the same bilayer thickness (24 Å) and coexist at compositions between 30 and 75 wt %, with a critical point at 62.2 wt % and 74 °C. Using osmotic pressure measurements, they showed that a true equilibrium between the two lamellar phases exists.⁴²

A systematic investigation of the rheological and structural properties of concentrated DDAB/EAN solutions ($[\text{DDAB}] > 68$ wt %) is presented here. It is worth noticing that the L_3 phase was observed in the DDAB/water system, but only as a metastable state in a very narrow region of the dilute regime ($[\text{DDAB}] \lesssim 1.5$ wt %).¹⁶ We find that the L_3 phase exists in a wide window in the DDAB/EAN (temperature–composition) phase diagram. At concentrations above ~80%, the system undergoes a first-order $L_3 - L_\alpha$ transition, confirmed independently by rheology, small angle neutron scattering, polarizing optical microscopy, and differential scanning calorimetry.

■ EXPERIMENTAL SECTION

Materials. DDAB (CAS 3282-73-3) of high purity was obtained from TCI America and used without further purification. EAN was purchased from Iolitec and dried by heating at 100 °C under a nitrogen atmosphere for several hours. This process reduces water contents to below levels detectable by Karl Fischer titration.⁴⁵ Deuterated EAN (dEAN) was prepared by mixing and heating (to 40 °C for 3 h) equimolar quantities of dry EAN and D₂O (Aldrich). The solution was then redried by heating the mixture to 90 °C under vacuum for 24 h and then remixed with D₂O. The process was repeated three times, resulting in about 2.5 of the amino hydrogens being replaced with deuterium, as ascertained by ¹H NMR.⁴¹

Phase Diagram. Surfactant solutions with compositions ranging from 68 to 95 wt % were prepared by weighing the designed amounts of DDAB and EAN in stoppered glass vials. The mixtures were homogenized by heating the vials to 100 °C (or 110 °C for samples with $[\text{DDAB}] > 90$ wt %) for 1 h. The samples were subsequently put in a thermostatted oil bath at the designed temperatures. Phase equilibrium of the lyotropic liquid crystal (LLC) phases was determined by visual inspection through crossed polarizers. Accurate determination of the type of LLC phase and phase boundaries was carried out by means of polarizing optical microscopy (POM), small angle neutron scattering (SANS), and oscillatory rheology.

Rheology. Small-amplitude oscillatory shear (SAOS) measurements were performed using a strain-controlled rheometer ARES G2 (TA Instruments) with $\gamma = 0.2$. To ensure homogeneity, the samples were heated at 100 °C before loading into the rheometer and then quenched to the desired testing temperature. Three type of dynamic tests were performed to characterize the $L_3 - L_\alpha$ transition: (1) temperature sweeps (in the range $15^\circ\text{C} \leq T \leq 120^\circ\text{C}$) at constant frequency (1 rad/s), with 10 min of equilibration at each temperature step (2 °C); (2) temperature ramps, down from 100 to 15 °C and up from 15 to 100 °C at 1 rad/s with a ramp rate of 3 °C/min (lowering the

cooling/heating rate further does not change the measured dynamic moduli); and (3) frequency sweeps, forward from 0.01 to 100 rad/s and backward from 100 to 0.01 rad/s. No hysteresis was observed when comparing forward and backward frequency sweeps. For the frequency sweeps, the samples were heated to 100 °C (or 110 °C for samples with $[\text{DDAB}] > 90$ wt %), after which they were cooled to the testing temperature, which was maintained for 1 h (to ensure equilibration) before the test. The cycle was repeated for each testing temperature.

Differential Scanning Calorimetry (DSC). DSC measurement was performed on the 85 wt % DDAB/EAN solution using a Q2000 differential scanning calorimeter (TA Instruments) at a rate of 3 °C/min. Two consecutive cooling/heating cycles were carried out in the temperature range: $20^\circ\text{C} < T < 90^\circ\text{C}$.

Small Angle Neutron Scattering (SANS). SANS was performed at the National Institute of Standards and Technology (NIST) in Gaithersburg, Maryland, on a 30 m beamline using neutrons with wavelength $\lambda = 6$ Å and wavelength spread $\Delta\lambda/\lambda = 0.11$. Solutions prepared with dEAN were used for SANS measurements. A negligible isotope effect was observed in the phase diagram when substituting EAN for dEAN, as shown below. Sample-to-detector distance was 1 m. Raw data were corrected for sample transmission, background radiation, sample thickness, and detector sensitivity using IGOR macros available from NIST.⁴⁶ Data were averaged azimuthally to obtain one-dimensional plots of intensity versus scattering wave vector.

Freeze-Fracture Transmission Electron Microscopy (FF-TEM). FF-TEM was performed by Randy A. Nessler at the University of Iowa's Central Microscopy Research Facilities using standard procedures of fast freezing, rupture, and carbon replication.⁴⁷ Acetone was used to wash the carbon replicas before imaging with a JEOL 2100F transmission electron microscope.

Ionic Conductivity Measurements. Conductivity measurements were carried out using a conductivity meter (CM, Oakton CON11). The CM was calibrated using KCl conductivity standards (Aldrich). Glass vials were filled with the samples and immersed in a thermostatted oil bath. The conductivity probe was submerged into the sample. All samples were thermally equilibrated at each temperature for 20 min prior to the measurements.

■ RESULTS AND DISCUSSION

Phase Behavior. The phase diagram of the DDAB/EAN system, for a broad composition range, is shown in Figure 1. A number of phases are identified: (1) a dilute phase containing monomeric units at $[\text{DDAB}] < 2$ wt %, (2) a pure (isotropic) sponge phase at $68 \text{ wt \%} < [\text{DDAB}] < 80 \text{ wt \%}$, (3) a miscibility gap (between 2 and 68 wt %) where the dilute and the L_3 phases coexist, (4) a (birefringent) lamellar phase at $[\text{DDAB}] > 80$ wt %, and (5) an unidentified (opaque, white) solid phase at very high concentrations and low temperatures. Upon cooling below ~30 °C, spontaneous and thermoreversible vesicle formation is observed in the dilute and semidilute regimes ($[\text{DDAB}] < 75$ wt %). These two regimes are discussed in a separate paper.⁴¹

The miscibility gap observed in the semidilute regime is analogous to that observed in the catanionic ternary system sodium dodecyl benzene sulfonate (SDBS)/DDAB/H₂O by Segota et al.^{48,49} A solid and a vesicular phase coexist in SDBS/DDAB/H₂O dilute solutions with surfactant mole ratios $0.05 < n_{\text{SDBS}}/n_{\text{DDAB}} < 0.5$. The coexistence region in DDAB/EAN solutions is $0.005 (2 \text{ wt \%}) < n_{\text{DDAB}}/n_{\text{EAN}} < 0.34 (68 \text{ wt \%})$. The

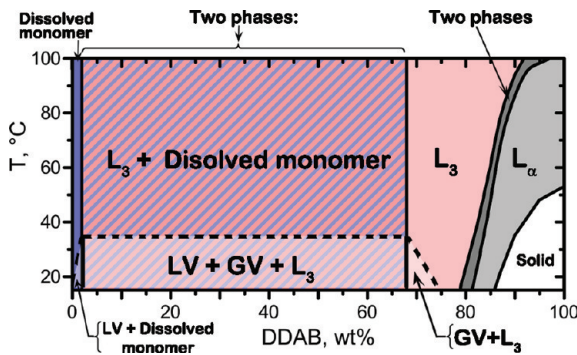


Figure 1. Phase diagram of DDAB/EAN. LV = large vesicles, GV = giant vesicles, L_3 = sponge phase, and L_α = lamellar phase. The solid region at the lower right corner corresponds to a nonidentified opaque phase. The dashed line marks the formation/destruction of both LV and GV.⁴¹

solid phase in the aqueous solutions may form due to the low solubility of DDAB in water, whereas the higher solubility of DDAB in EAN leads to the formation of swollen bilayers (L_3 or L_α) instead of a precipitate.

Here, we focus on the $L_3 - L_\alpha$ transition occurring at $[DDAB] > 80$ wt %. This transition was mapped using dynamic shear rheology and birefringence observations. Figure 2 shows the elastic and viscous moduli as a function of temperature for DDAB concentrations of 68 wt % and above. For concentrations below 80 wt %, G'' increases monotonically as the temperature is decreased from 120 to 15 °C, whereas G' is negligible and constant throughout the temperature range. These samples are not birefringent when observed through crossed polarizers or by POM. At compositions $[DDAB] > 80$ wt %, a sharp increase in both G' and G'' is observed at a temperature marked as T_1 in Figure 2. The moduli increase until the system reaches the temperature T_2 , below which a second regime of monotonic growth is observed. These samples show high fluidity and no birefringence for $T > T_1$, but are gel-like and birefringent for temperatures below T_2 . Figure 3 show these transitions for the 85 wt % DDAB/EAN sample as observed through crossed polarizers and by POM.⁵⁰

Temperatures T_1 and T_2 as determined by rheology for both DDAB/EAN and DDAB/dEAN systems are plotted versus DDAB mole fraction in Figure 4. The concentration scales in weight percent for both systems are included to ease direct comparison with other plots in the paper. The region between T_1 and T_2 corresponds to the $L_3 - L_\alpha$ transition where a macroscopic coexistence of both phases is observed through crossed polarizers (Figure 3). The typical Maltese cross texture corresponding to the lamellar (L_α) phase at $T < T_2$ are evident in the POM micrographs (Figure 3).⁵⁰ The absence of birefringence, the low viscosity, and the low concentration dependence of the viscosity are first indications of the existence of a sponge (L_3) phase at $T > T_1$.^{15,51} It is worth mentioning that the L_3 phase is typically observed in ternary surfactant/cosurfactant/water systems within narrow regions of solubility.^{52–54} In contrast, DDAB/EAN solutions form a stable L_3 phase in a wide range of compositions and temperatures.

Temperature Hysteresis of the $L_3 - L_\alpha$ Transition. Figure 5 shows DSC traces for the 86 wt % DDAB/EAN solution using heating/cooling rates of 3 °C/min. A cooling process followed by a heating process was performed in the range 20 °C < $T < 90$ °C. The transition from L_α to L_3 is marked by the exothermic peak

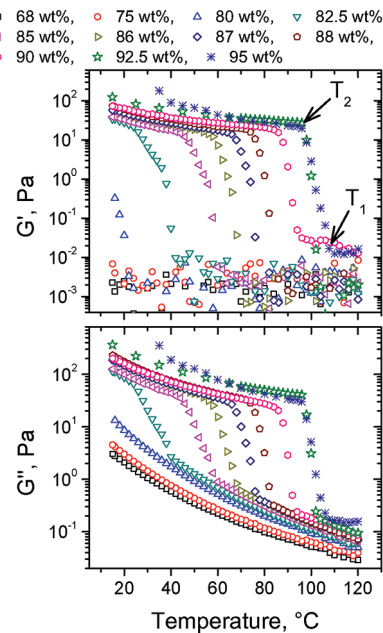


Figure 2. Dynamic temperature sweeps for DDAB/EAN solutons with 10 min of equilibration at each temperature step (2 °C). The strain and frequency used are 0.2 and 1 rad/s, respectively. Temperatures T_1 and T_2 delineate the $L_3 - L_\alpha$ transition.

near 60 °C, which evidences the melting of the hydrocarbon chains within the bilayers. This results in a reduction of the membrane bending constant, which leads to a reduction in the free energy via minimizing the membrane curvature, and the formation of a bicontinuous (sponge) surface.⁵⁵ The upper (cooling) DSC curve shows a slight displacement of the $L_3 - L_\alpha$ transition, due in part to supercooling and in part to instrumental hysteresis attributable to the temperature scan rate. Both the transition temperature and the thermal hysteresis are mirrored by the mechanical dynamic temperature ramp shown in Figure 5. Notice that no hysteresis is observed in the loss modulus, but the supercooling of the L_3 phase (before transforming to the lamellar phase) is evidenced by the sharp increase in G' at ~62 °C upon cooling. In contrast, the transition from L_α to L_3 is more gradual, as observed in the G' ramp-up plot.

The peak in the DSC traces indicates that the $L_3 - L_\alpha$ transition is of first order, which suggests that the equilibrium phases at the transition (Figure 3) do not have the same composition. Therefore, the surfactant volume fraction shows a jump, ϕ_3 to ϕ_ω when going from L_3 to L_ω resulting in the phase coexistence observed in Figure 3.

Evolution of the Viscoelastic Properties during the $L_3 - L_\alpha$ Transition. The transition from a low viscosity liquid to a flow-arrested state, which is obvious to the naked eye (see Figure 3 and the ref 50), is further studied with SAOS. Figure 6 gives the dynamic moduli and $\tan \delta$ versus frequency for the 85 wt % DDAB/EAN solution at different temperatures covering the L_3 region, the transition, and the L_α region (as indicated in the inset). At temperatures within the L_3 region ($T \geq 62$ °C) the slopes of $\log G'$ and $\log G''$ vs $\log \omega$ are 2 and 1, respectively, which are typical values for viscoelastic liquids in the terminal region.⁵⁶ This low viscosity is typical of the L_3 phase because of the easy reorientation or creation/destruction of the membrane to relieve stresses in slight departures from equilibrium.³ Unlike the sponge phase, the lamellar phase is not fluid; therefore its

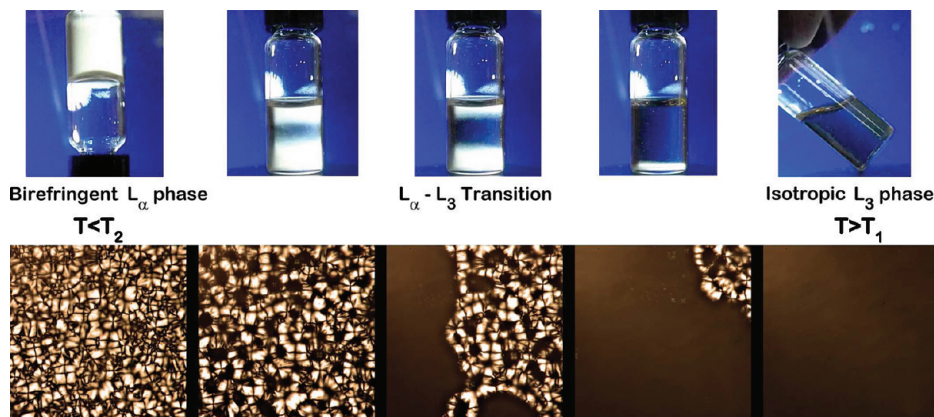


Figure 3. Birefringence change during the L_3 – L_α transition for the 85 wt % DDAB/EAN solution observed through cross polarizers (upper row) and by POM (lower row). Upper row: The solution behaves as a birefringent gel at $T < T_2$ and as an isotropic Newtonian liquid at $T > T_1$ (see Figure 2). Lower row: Maltese cross texture (characteristic of the lamellar phase) disappear upon heating. See ref 50 for links to Quicktime movies.

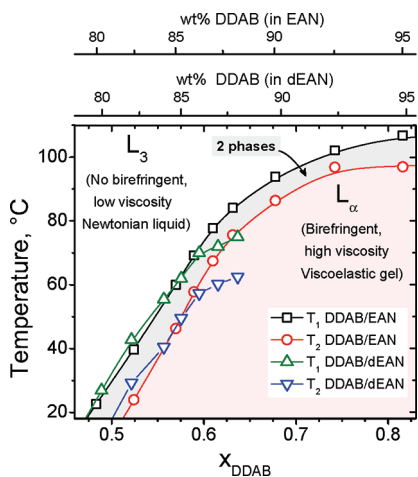


Figure 4. Phase behavior of DDAB/EAN and DDAB/dEAN in the concentrated regime. Temperatures T_1 and T_2 are determined by rheological measurements (Figure 2), visual inspection between backlit crossed polarizers, and POM (Figure 3). The concentration scales in weight percent for both systems are included to facilitate comparison with other plots in the paper.

viscosity is higher and dependent on mobility defects on the texture or structural length scales.

The transition from liquidlike to solidlike behavior (gel point) is determined as the temperature where the power law dependences for both G' and G'' become equal to an exponent of ~ 0.5 , over more than a decade of frequency, which is the typical signature of gelation.⁵⁷ This occurs at ~ 60 °C for the 85 wt % DDAB/EAN solution (see Figure 6) and corresponds to the transition line between L_3 and the two-phase region in the phase diagram (Figure 4).

The transition to L_α is accompanied by a further decrease in the slopes of $\log G'(\omega)$ and $G''(\omega)$ at low frequencies, both being equal and less than 0.05. Moreover, the elastic modulus is at least 3 orders of magnitude larger than in the L_3 phase at the same concentration, which is also observed in the temperature sweeps (Figure 2). It is noticeable that even when the elasticity is enhanced after the L_3 – L_α transition, G' never exceeds G'' , and both moduli show the same dependence on ω . This behavior is

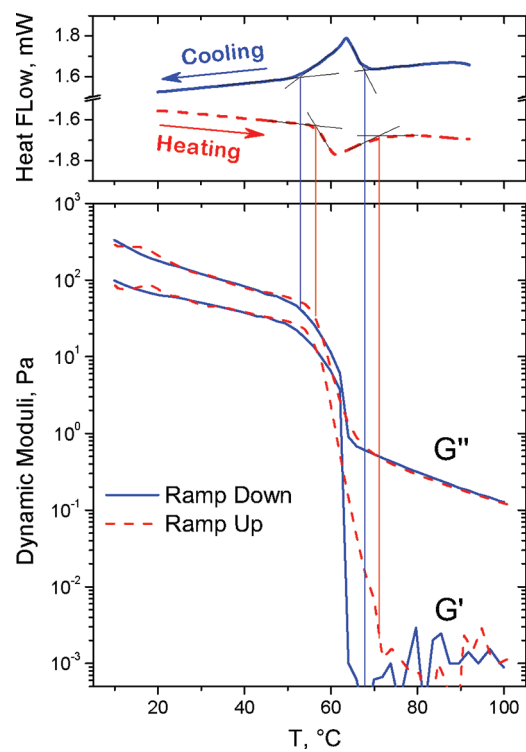


Figure 5. DSC thermograms and dynamic temperature ramp for the 85 wt % DDAB/EAN solution. L_3 – L_α transition is marked by exothermic (cooling) and endothermic (heating) DSC peaks and by an increase in G' and G'' . Temperature hysteresis, due to the L_3 supercooling during the ramp-down tests, is mirrored in both tests.

characteristic of a “weak gel” and has been observed in other surfactant systems.^{58,59} At temperatures within the transition region (60 and 62 °C), G' and G'' exhibit intermediate rheological behavior between L_α and L_3 , as expected.

Structural Analysis during the L_3 – L_α Transition: SANS Studies. To enhance neutron contrast between the surfactant bilayer and the solvent, the DDAB solutions for SANS were prepared in dEAN. By substituting EAN for dEAN, a small isotope effect in the phase diagram was observed in compositions [DDAB] < 86 wt % (see Figure 4). A stronger effect was observed

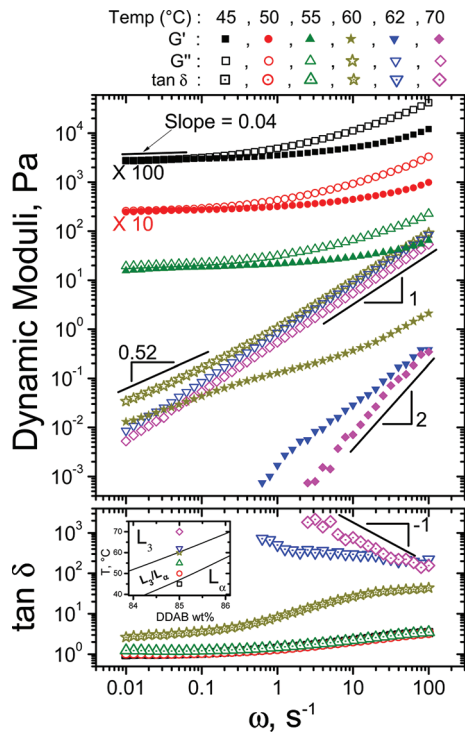


Figure 6. Dynamic frequency sweeps at strain of 0.2 for the 85 wt % DDAB/EAN solution at various temperatures spanning from the L_3 region to the L_α region. The inset gives a detail of the phase diagram with the temperatures tested indicated with symbols. Dynamic moduli at 45 and 50 °C are multiplied by 100 and 10, respectively, for clarity.

at compositions $[DDAB] > 86$ wt %, which were avoided in SANS experiments. Figure 7 gives the SANS profiles at 25 °C for the DDAB/EAN system with different compositions covering the three zones in the phase diagram (see inset in Figure 7). The peak observed in all SANS profiles reveals the characteristic length corresponding to the interlayer spacing. A transition from a broad peak to a narrow peak as well as a shift in the peak position are observed upon increasing the composition from 80 to 82 wt %, which is the composition range over which the L_3 – L_α transition takes place at 25 °C (see Figure 4).

The Teubner–Strey (TS) model⁶⁰ was used to fit the SANS data. The TS model, originally introduced to represent the structure of microemulsions, has the following functional form:

$$I(q) = \frac{1}{a_2 + c_1 q^2 + c_2 q^4} \quad (1)$$

where $I(q)$ is the scattering intensity, and a_2 , c_1 , and c_2 are composition-dependent coefficients. The correlation length, ξ , and the d -spacing (characteristic of a domain size or periodicity) are

$$\begin{aligned} \xi &= \left[\frac{1}{2} \left(\frac{a_2}{c_2} \right)^{1/2} + \frac{1}{4} \frac{c_1}{c_2} \right]^{-1/2} \\ d &= 2\pi \left[\frac{1}{2} \left(\frac{a_2}{c_2} \right)^{1/2} - \frac{1}{4} \frac{c_1}{c_2} \right]^{-1/2} \end{aligned} \quad (2)$$

The amphiphilicity factor, $f_a = c_1/(4a_2c_2)^{1/2}$, represent the amphiphile strength that dictates the microstructure.⁶¹ For example, the ordered lamellar phase corresponds to $f_a = -1$, whereas

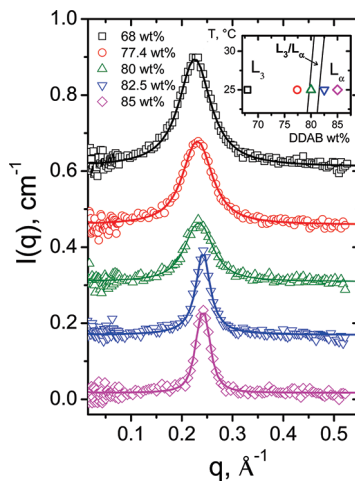


Figure 7. SANS profiles measured at 25 °C for DDAB/dEAN solutions with various concentrations spanning from the L_3 region to the L_α region. The inset gives a detail of the phase diagram with the concentration tested indicated with symbols. Solid lines are fits to the Teubner–Strey model (eq 1).⁶⁰ Curves are shifted vertically for clarity.

the disordered phase (i.e., with null correlation) corresponds to $f_a = 1$.

We used the TS model to obtain the correlation length and the quasi-periodic d -spacing characterizing the sponge phase and the lamellar phases. The solid lines in Figure 7 are the model fits. Both ξ and d are given as a function of DDAB composition in Figure 8. Notice that the correlation length in the sponge phase is comparable to the thickness of the bilayer (2.1 nm⁴¹), and it doubles for the lamellar state, indicating a more ordered state. In contrast, the d -spacing decreases for the L_3 – L_α transition, evidencing that the bilayers are slightly more packed in the lamellar state.

The amphiphilicity factor is given in Figure 8 as a function of DDAB composition. The fact that all these values are very close to the lower limit of f_a (i.e., -1), indicates that both L_3 and L_α are ordered phases. However the decrease at the L_3 – L_α transition (from $f_a \sim -0.955$ to $f_a \sim -0.985$) confirms that the L_α phase is slightly more ordered than the L_3 phase. The thickness of the EAN channels, calculated with $\delta_{EAN} = d - \delta$ (see inset in Figure 9), shows a sharp decrease at the L_3 – L_α transition, indicating a jump in density, which is typical of a first-order phase transition, as verified by DSC (Figure 5).

The TS model assumes the pair correlation function,

$$g(r) = \frac{d}{2\pi r} \exp\left(-\frac{r}{\xi}\right) \sin\left(\frac{2\pi r}{d}\right) \quad (3)$$

which combines two well-known features of microemulsion: namely, the alternation of water and oil containing domains and the absence of a long-range order.⁶¹ In this case, the two domains are the EAN channels and the interior of surfactant bilayers, respectively (see inset in Figure 9). Figure 9 shows the pair correlation function, $g(r)$, as a function of the distance, r , for the 77.4 and 85 wt % DDAB/dEAN solution at 25 °C. This shows that the correlation vanishes at $r > \sim 30$ Å in the L_3 phase, but in the L_α phase, the correlation is still evident at $r \sim 58$ Å. This is reflected in the fitted value of ξ (see Figure 8).

Figure 10 shows that the periodicity of the L_3 phase varies linearly with the inverse of the DDAB volume fraction, which

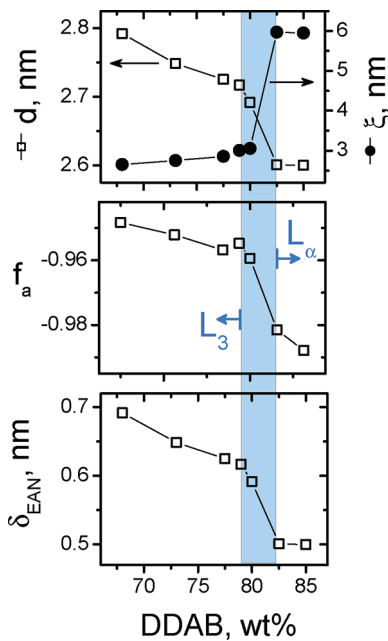


Figure 8. Structural parameters versus DDAB concentration. Correlation length (ξ), intermembrane spacing (d), amphiphilicity factor (f_a), and EAN channel thickness (δ_{EAN}) obtained by fitting SANS data (at 25 °C) with the Teubner–Strey model (eq 1). The shaded area represents the L_3 – L_α transition.

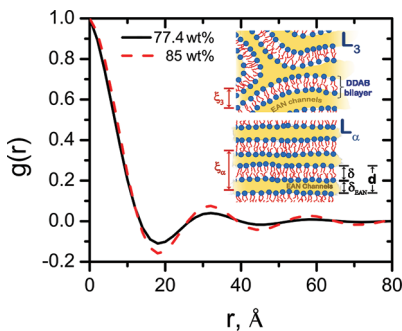


Figure 9. Pair correlation function for the 77.4 and 85 wt % DDAB/dEAN solutions at 25 °C computed with eq 3, using ξ and d obtained from the SANS data (Figure 7). Inset shows schematics of the sponge phase (observed in 77.4 wt % DDAB/dEAN) and the lamellar phase (observed in 85 wt % DDAB/dEAN).

indicates that this phase follows the expected dilution law. The same behavior was reported previously for the cetylpiridinium/hexano-/brine system.^{8,9} The universal dilution law results from the fact that the topology of the membrane is unaltered over the volume fraction range for which the law is upheld (i.e., pure swelling occurs upon increasing the surfactant concentration). Such a law has only been observed in two liquid crystal phases: namely, L_3 and L_α .^{9,62} Unfortunately, we do not have enough data to confirm the dilution law in the L_α phase.

The asymptotic scattering at $q > 2\pi/d$ is analyzed from the log–log scale plot of the scattering curves. Figure 11a shows the scattering in absolute units for a sample in the L_3 region (68 wt % DDAB) and a sample in the L_α region (85 wt % DDAB). For both samples, the scattering intensity at $q > 0.3 \text{ Å}^{-1}$ decays with a slope of ~ -2 (the fitted slopes are -2.23 ± 0.14 and 1.94 ± 0.18

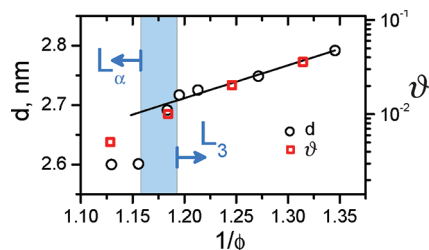


Figure 10. Dilution law and obstruction factor for DDAB/EAN solutions at 25 °C determined from SANS and ionic conductivity measurements, respectively. The shaded area represents the L_3 – L_α transition.

for 68 and 85 wt % DDAB, respectively). This indicates that both phases have similar local bilayer structure, very much like those observed in dilute aqueous L_3 phases.^{21,51,63} Using FF-TEM, we further verify that the structures are bicontinuous (sponge) in the L_3 phase region (Figure 11b) and lamellar in the L_α region (Figure 11c).

Ionic Conductivity of the L_3 and L_α Phases. Due to high ionic dissociation, EAN is a good conductor of electric charge,⁶⁴ whereas the DDAB membrane acts as an electric insulator. Hence, conductivity measurements indirectly probe the membrane structure. Strey and co-workers⁶³ showed that both the L_3 and the L_α phases can be identified by dc conductivity, σ . Figure 12 shows the temperature dependence of the ionic conductivity and the viscosity for EAN and DDAB/EAN solutions. The conductivity at the maximum swelling (~ 68 wt %) is 2 orders of magnitude lower than the pure EAN. This contrasts with the modest reduction in conductivity observed in aqueous dilute L_3 phases.^{63,65–68}

The decrease in σ is due to two main effects:⁶³ (1) the trivial decrease of the ion concentration due to the presence of insulating units (which explains the huge reduction in σ for the concentrated DDAB/EAN solutions) and (2) the obstruction caused by structural aggregates, that is, the bilayer membrane. Accordingly, the obstruction factor, defined as⁶³

$$\vartheta \equiv \frac{\sigma}{(1 - \phi)\sigma_{EAN}} \quad (4)$$

is sensitive to the topological structure of the membrane. The term $(1 - \phi)$ accounts for the fact that the effective volume for ion transport is the solvent volume.

Activation Energies of Conductivity and Viscosity. Weingartner et al.⁶⁴ reported the ionic conductivity (obtained from complex permittivity measurements using four different techniques) and the viscosity (measured by a falling ball viscosimeter) for EAN at different temperatures. Their results are in agreement to those reported here (see Figure 12). To describe the temperature dependence of σ and η , they used the Arrhenius expressions:

$$\begin{aligned} \sigma &= \sigma_0 \exp[-E_{a\sigma}/RT] \\ \eta &= \eta_\infty \exp[E_{a\eta}/RT] \end{aligned} \quad (5)$$

where R is the gas constant. The activation energies, $E_{a\sigma}$ and $E_{a\eta}$, and the prefactors, σ_0 and η_∞ , reported by Weingartner et al.⁶⁴ are given in Table 1.

We observed that eqs 5 do not describe the temperature dependence of σ and η throughout the temperature range studied here. This is evident by the curvature observed in the Arrhenius plots given in Figure 12 (eqs 5 generate straight lines). The same

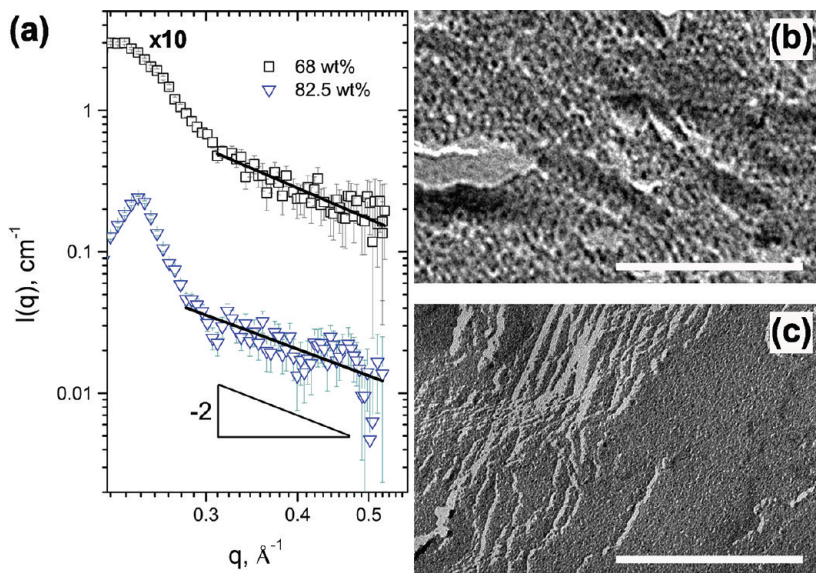


Figure 11. (a) SANS profiles (plotted in log–log scale) for 68 and 85 wt % DDAB/dEAN solutions measured at 25 °C. SANS data are shifted vertically for clarity. (b, c) Freeze-fracture TEM images of the 68 and 85 wt % DDAB/dEAN solutions, respectively. The scale bar in both images is 200 nm.

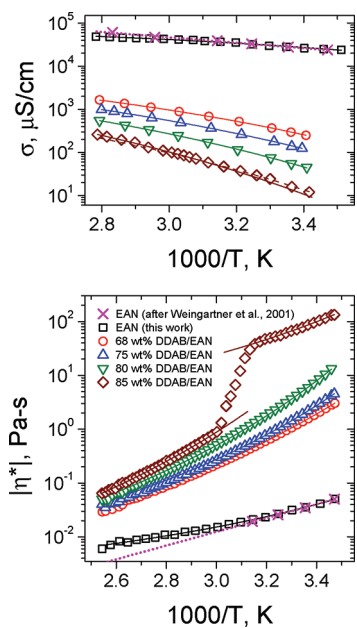


Figure 12. (a) Conductivity and (b) viscosity as a function of temperature and concentration for EAN and DDAB/EAN solutions (symbols correspond to the same compositions in both plots). Solid lines are fits to the VTF model (eq 6). The dashed line corresponds to the L_α phase in the 68 wt % solution, whereas solid lines correspond to the L_3 phase. Crosses are data reported in ref 64, and dotted lines are fits to Arrhenius equations (eq 5) for those data.

behavior has been observed in other ionic liquid and ionic-liquid-containing systems.^{69–79} The temperature dependence of both σ and η for those systems is commonly described by the Vogel–Fulcher–Tammann (VTF) equation,^{80–82}

$$\begin{aligned} \sigma &= \sigma_0 \exp[B_\sigma/(T - T_0)] \\ \eta &= \eta_\infty \exp[B_\eta/R(T - T_0)] \end{aligned} \quad (6)$$

where η_∞ is the limiting viscosity at high temperatures, σ_0 is a prefactor, and the constants B_η and B_σ are related to the entropic barrier of molecular motion⁸³ and of conduction,⁷⁷ respectively. The latter parameters can be used to obtain pseudoactivation energies: $E_{a\sigma} = -RB_\sigma$ and $E_{a\eta} = RB_\eta$. T_0 is the Vogel temperature at which the viscosity becomes infinite and the conductivity drops to zero.

Solid lines in Figures 12 and 13 are fits to eq 6 for EAN and DDAB/EAN solutions. The VTF parameters are given in Table 1. Notice that the fitted Vogel temperatures for EAN (for both σ and η) are very close to the EAN glass transition temperature ($T_{g,EAN} = -95$ °C) measured calorimetrically.⁸⁴ Given that the electrical conduction in the L_3 phase is exclusively through the ionic liquid and that we do not have information on the glass transition of the DDAB/EAN solutions, we arbitrarily set $T_0 = T_{0,EAN}$ for all the fittings. For the solutions that undergo L_3-L_α transition, we fit each temperature range (corresponding to each phase) separately.

The activation energy for viscosity is considerably larger than for conductivity (see Table 1) for EAN and the solutions. This behavior is typical of other molten salts and is related to the high ionicity of EAN.^{64,85} Figure 14 shows that both activation energies (in the L_3 phase) increase with the concentration. In addition, they follow similar dependencies on concentration, and they are linearly related to each other (see inset in Figure 14a). This suggests that the decrease in conductivity is mostly due to hindering of molecular motion imposed by the membrane structure.

A counterintuitive result is the decrease in $E_{a\eta}$ with increasing concentration for the L_α phase (Figure 14b), which indicates that the height of the potential barrier for viscous flow is smaller as we add more surfactant. One possible scenario to explain this is that the lamellas align easily in the flow direction at higher concentrations. Then the viscous resistance is dominated by the sliding of the lamellas over the EAN channels, which explains the fact that the value $E_{a\eta}$ approaches that of pure EAN as [DDAB] increases.

Table 1. VTF Parameters of Viscosity and Conductivity for EAN and DDAB/EAN Solutions

sample (phase)	η_∞ , Pa-s	$E_{a\eta}$, kJ/mol	$T_{0\eta}$, K	σ_0 , $\mu\text{S}/\text{cm}$	$E_{a\sigma}$, kJ/mol	$T_{0\sigma}$, K
EAN	9.74×10^{-4}	3.43	183	1.40×10^5	1.54	181
	1.81×10^{-6} ^a	24.5 ^a		4.10×10^6 ^a	12.4 ^a	
68 wt % DDAB (L_3)	4.18×10^{-4}	7.54	181	4.37×10^4	4.82	181
75 wt % DDAB (L_3)	4.03×10^{-4}	8.42	181	4.21×10^4	5.49	181
80 wt % DDAB (L_3)	1.74×10^{-4}	10.1	181	4.45×10^4	6.46	181
82.5 wt % DDAB (L_3)	1.01×10^{-4}	11.1	181			
82.5 wt % DDAB (L_α)	0.13	6.08	181			
85 wt % DDAB (L_3)	8.55×10^{-5}	11.7	181	6.96×10^4	8.24	181
85 wt % DDAB (L_α)	0.43	5.22	181	2.91×10^4	7.20	181
86 wt % DDAB (L_3)	7.35×10^{-5}	12.1	181			
86 wt % DDAB (L_α)	0.49	5.32	181			
87 wt % DDAB (L_3)	7.24×10^{-5}	12.2	181			
87 wt % DDAB (L_α)	0.86	4.85	181			
88 wt % DDAB (L_3)	5.31×10^{-5}	12.7	181			
88 wt % DDAB (L_α)	0.93	4.93	181			
90 wt % DDAB (L_3)	5.05×10^{-5}	12.9	181			
90 wt % DDAB (L_α)	1.47	4.49	181			
92 wt % DDAB (L_3)	3.97×10^{-5}	13.6	181			
92 wt % DDAB (L_α)	7.69	2.32	181			

^a Fitting parameters to Arrhenius expressions (eqs 5). After Weingartner et al.⁶⁴

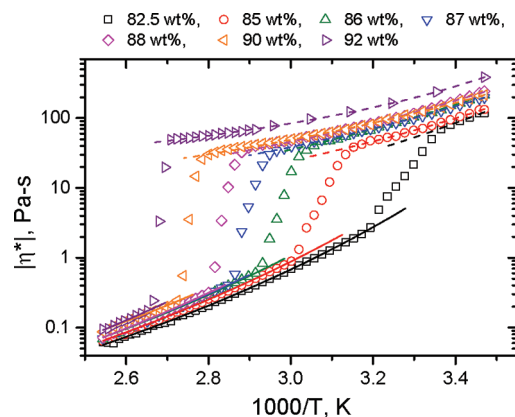


Figure 13. Viscosity as a function of temperature and concentration for concentrated DDAB/EAN solutions. Solid and dashed lines are fits to the VTF model (eq 6) corresponding to the L_3 phase and to the L_α phase, respectively.

Obstruction Factor. A direct consequence of the swelling of the L_3 phase is a decrease in the obstruction factor (eq 4) with the surfactant volume fraction.^{51,63,68} Figure 10 shows that both the repeating distance (a geometrical parameter) and the obstruction factor (a topological parameter) increase monotonically with $1/\phi$ for the L_3 phase. However, the increase is linear for d and exponential for ϑ , which suggests an exponential dependence between these two parameters, that is, $\vartheta \sim e^d$.

Figure 15a shows the obstruction factor as a function of temperature and concentration. The observed growth in ϑ with temperature may be due to an increment in the number of pores in the bicontinuous membrane, which indicates an increase in the mean curvature induced by thermal energy. Using eqs 4 and 6, the obstruction factor can be described

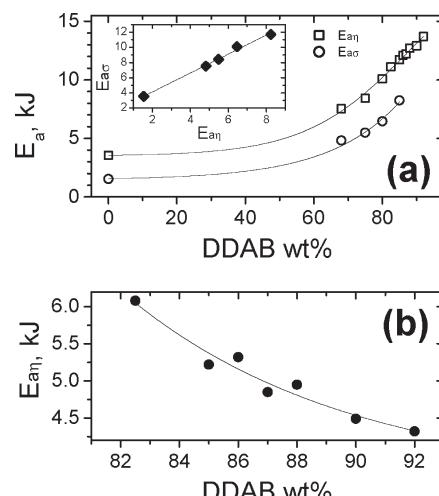


Figure 14. (a) Activation energies of conductivity and viscosity for EAN and DDAB/EAN solutions in the L_3 phase obtained by fittings to eqs 6. Inset shows the linear relation between $E_{a\sigma}$ and $E_{a\eta}$. (b) Activation energy of viscosity for DDAB/EAN solutions in the L_α phase. Lines are to guide the eye.

with the VTF expression

$$\vartheta = \vartheta_0 \exp[-E_{a\vartheta}/R(T - T_0)] \quad (7)$$

with $\vartheta_0 = \sigma_0/(1 - \phi)\sigma_{0,\text{EAN}}$ and $E_{a\vartheta} = E_{a\sigma} - E_{a\sigma,\text{EAN}}$.

The obstruction factor for the system studied here is remarkably lower than $2/3$, which is the expected value for the sponge phase.⁶³ This could be due to the solvation of the bilayer surface.⁸⁶ Binding of EAN ions to the membrane surface would reduce the molecular mobility and, hence, the conductivity. Because of the very high surfactant concentration, this effect may be

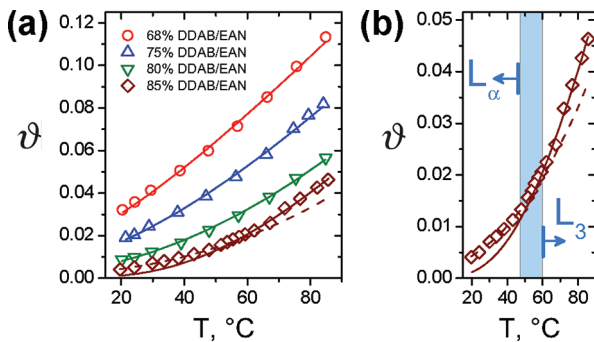


Figure 15. (a) Obstruction factor as a function of temperature and concentration for DDAB/EAN solutions. (b) ϑ versus temperature for the 85 wt % DDAB/EAN solution showing the L_3 – L_α transition. Lines are plots of eq 7 using the parameters given in Table 1 (solid lines correspond to the L_3 phase, and dashed lines, to the L_α phase).

considerable for our samples and could explain the overall low conductivities.

The solid lines in Figure 15a are plots of eq 7 using the parameters given in Table 1. $E_{a\vartheta}$ in eq 7 represents the energy barrier of creation of defects (pores) in the membrane, which facilitate ion transport. $E_{a\vartheta}$ could also include the binding energy of ions from EAN at the membrane/liquid interface. The L_3 – L_α is marked by a continuous change in the mode of growth of the obstruction factor, as indicated with the two fits to eq 7 (solid and dashed lines in Figure 15b). It is well-known that the conductivity in the lamellar phase is due to defects such as handles connecting the membranes.⁸⁷ Upon heating, these holes become more numerous and more interconnected and eventually become part of the bicontinuous L_3 phase. This results in less tortuosity of the conduction path through the spongelike membrane;⁸⁸ hence, the increase in ϑ .

Finally, the stable L_3 phase for DDAB in an RTIL (EAN) has not analog in aqueous solutions, where only a metastable L_3 phase has been reported over a narrow range of compositions (<1.5 wt %). In EAN, the L_3 phase appears at much higher compositions. That much higher surfactant concentration we required to generate the L_3 phase in EAN is not surprising, given the much lower solvophobic effect as compared with aqueous solutions. One might speculate that the extreme shield of the ionic head groups in RTILs coupled with weaker solvophobic interactions leads to significantly lower membrane rigidity, and thus, significantly higher concentrations are required to stabilize the lamellar phase. A more complete molecular thermodynamics study of self-assembly in ILs is warranted to fully understand the microphase separation.

CONCLUSIONS

We have studied the L_3 – L_α transition in the DDAB/EAN system using a wide range of experimental probes, including viscosity, elasticity, conductivity, phase behavior, birefringence, and microstructure. The weaker solvophobic effect acting in EAN, compared with water, leads to the formation of a stable DDAB L_3 phase over a wide range of compositions. This fact makes the DDAB/EAN system an excellent candidate for applications of the sponge phase because this phase exists only in very narrow composition windows in aqueous systems. To our knowledge, this is the first report of the L_3 phase in an ionic liquid. We have identified the L_3 phase as an isotropic (nonbirefringent),

low-viscosity Newtonian fluid with relatively small structural correlation length. This phase does not undergo topological transformations upon dilution, as evidenced by the fulfillment of a universal dilution law. A first-order sponge-to-lamellar transition was characterized by an extra-heat flow peak in the DSC plots and a sharp increase in the dynamic moduli. This transition was also evidenced by the appearance of birefringent textures corresponding to the L_α observed by POM and an increase in the correlation length measured by SANS. Of great interest is to understand the flow behavior of the system near the phase transition. We are particularly interested in studying the shear-induced structural transitions of the L_3 phase and the transient rheology and morphology of the L_α phase during flow.

W Web Enhanced Feature. Two movies featuring the change in birefringence and the appearance of Maltese crosses upon the L_3 – L_α transition are available in the HTML version of the paper.

AUTHOR INFORMATION

Corresponding Author

*E-mail: wagnernj@udel.edu.

ACKNOWLEDGMENT

We acknowledge Professor Ulf Olsson (Lund) for helpful comments. This manuscript was prepared under cooperative agreement 70NANB7H6178 from the National Institute of Standards and Technology (NIST), US Department of Commerce. The statements, findings, conclusions, and recommendations are those of the authors and do not necessarily reflect the views of NIST or the US Department of Commerce.

REFERENCES

- (1) Cates, M. E.; Roux, D.; Adelman, D.; Milner, S. T.; Safran, S. A. *Europhys. Lett.* **1988**, *5*, 733–739.
- (2) Porte, G. *Curr. Opin. Colloid Interface Sci.* **1996**, *1*, 345–349.
- (3) Snabre, P.; Porte, G. *Europhys. Lett.* **1990**, *13*, 641–645.
- (4) Antelmi, D.; Kékicheff, P.; Richetti, P. *J. Phys. II France* **1995**, *5*, 103–112.
- (5) Alfons, K.; Engstrom, S. *J. Pharm. Sci.* **1998**, *87*, 1527–1530.
- (6) Drummond, C. J.; Fong, C. *Curr. Opin. Colloid Interface Sci.* **1999**, *4*, 449–456.
- (7) Chang, J. H.; Shim, C. H.; Kim, B. J.; Shin, Y.; Exarhos, G. J.; Kim, K. J. *Adv. Mater.* **2005**, *17*, 634–637.
- (8) McGrath, K. M.; Dabbs, D. M.; Yao, N.; Aksay, I. A.; Gruner, S. M. *Science* **1997**, *277*, 552–556.
- (9) McGrath, K. M.; Dabbs, D. M.; Yao, N.; Edler, K. J.; Aksay, I. A.; Gruner, S. M. *Langmuir* **2000**, *16*, 398–406.
- (10) Antonietti, M. *Philos. Trans. R. Soc. A* **2006**, *364*, 2817–2840.
- (11) Lindblom, G.; Rilfors, L. *Biochim. Biophys. Acta* **1989**, *988*, 221–256.
- (12) Lang, J. C.; Morgan, R. D. *J. Chem. Phys.* **1980**, *73*, 5849–5861.
- (13) Mitchell, D. J.; Tiddy, G. J. T.; Waring, L.; Bostock, T.; McDonald, M. P. *J. Chem. Soc. Faraday Trans. 1* **1983**, *79*, 975–1000.
- (14) Maldonado, A.; Urbach, W.; Ober, R.; Langevin, D. *Phys. Rev. E* **1996**, *54*, 1774–1778.
- (15) Lynch, M. L.; Spicer, P. T. *Bicontinuous Liquid Crystals*; Taylor and Francis: Boca Raton, 2005; Vol. 127.
- (16) Dubois, M.; Zemb, T. *Langmuir* **1991**, *7*, 1352–1360.
- (17) Porte, G.; Appell, J.; Bassereau, P.; Marignan, J. *J. Phys. (Paris)* **1989**, *50*, 1335–1347.
- (18) Skouri, M.; Marignan, J.; Appell, J.; Porte, G. *J. Phys. II* **1991**, *1*, 1121–1132.

- (19) Porte, G.; Delsanti, M.; Billard, I.; Skouri, M.; Appell, J.; Marignan, J.; Debeauvais, F. *J. Phys. II* **1991**, *1*, 1101–1120.
- (20) Morse, D. C. *Phys. Rev. E* **1994**, *50*, R2423–R2426.
- (21) Gazeau, D.; Bellocq, A. M.; Roux, D.; Zemb, T. *Europhys. Lett.* **1989**, *9*, 447–452.
- (22) Le, T.; Olsson, U.; Wennerstrom, H.; Schurtenberger, P. *Phys. Rev. E* **1999**, *60*, 4300–4309.
- (23) Welton, T. *Chem. Rev.* **1999**, *99*, 2071–2084.
- (24) Rogers, R. D.; Seddon, K. R. *Science* **2003**, *302*, 792–793.
- (25) Freemantle, M. *An Introduction to Ionic Liquids*; Royal Society of Chemistry Publishing: Cambridge, 2010.
- (26) Dupont, J.; de Souza, R. F.; Suarez, P. A. Z. *Chem. Rev.* **2002**, *102*, 3667–3692.
- (27) van Rantwijk, F.; Sheldon, R. A. *Chem. Rev.* **2007**, *107*, 2757–2785.
- (28) Pârvulescu, V. I.; Hardacre, C. *Chem. Rev.* **2007**, *107*, 2615–2665.
- (29) Han, X.; Armstrong, D. W. *Acc. Chem. Res.* **2007**, *40*, 1079–1086.
- (30) Walden, P. *Bull. Acad. Imper. Sci. (St. Pétersbourg)* **1914**, *85*, 1800–1801.
- (31) Evans, D. F.; Yamauchi, A.; Roman, R.; Casassa, E. Z. *J. Colloid Interface Sci.* **1982**, *88*, 89–96.
- (32) Evans, D. F.; Yamauchi, A.; Wei, G. J.; Bloomfield, V. A. *J. Phys. Chem.* **1983**, *87*, 3537–3541.
- (33) Evans, D. F.; Kaler, E. W.; Benton, W. J. *J. Phys. Chem.* **1983**, *87*, 533–535.
- (34) Araos, M. U.; Warr, G. G. *J. Phys. Chem. B* **2005**, *109*, 14275–14277.
- (35) Greaves, T. L.; Weerawardena, A.; Fong, C.; Drummond, C. J. *J. Phys. Chem. B* **2007**, *111*, 4082–4088.
- (36) Hao, J.; Zemb, T. *Curr. Opin. Colloid Interface Sci.* **2007**, *12*, 129–137.
- (37) Greaves, T. L.; Drummond, C. J. *Chem. Soc. Rev.* **2008**, *37*, 1709–1726.
- (38) Araos, M. U.; Warr, G. G. *Langmuir* **2008**, *24*, 9354–9360.
- (39) Fumino, K.; Wulf, A.; Ludwig, R. *Angew. Chem.* **2009**, *48*, 3184–3186.
- (40) Tadros, T. F. *Applied Surfactants: Principles and Applications*; Wiley-VCH: Weinheim; Great Britain, 2005.
- (41) López-Barrón, C. R.; Basavaraj, M.; Wagner, N. J. *J. Am. Chem. Soc.*, in revision.
- (42) Zemb, T.; Belloni, L.; Dubois, M.; Marcelja, S. *Prog. Colloid Polym. Sci.* **1992**, *89*, 33–38.
- (43) Zemb, T.; Gazeau, D.; Dubois, M.; Gulik-Krzywicki, T. *Europhys. Lett.* **1993**, *21*, 759–766.
- (44) Dubois, M.; Zemb, T.; Fuller, N.; Rand, R. P.; Parsegian, V. A. *J. Chem. Phys.* **1998**, *108*, 7855–7869.
- (45) Atkin, R.; Warr, G. G. *J. Phys. Chem. C* **2007**, *111*, 5162–5168.
- (46) Kline, S. R. *J. Appl. Crystallogr.* **2006**, *39*, 895–900.
- (47) Gulik-Krzywicki, T. *Curr. Opin. Colloid Interface Sci.* **1997**, *2*, 137–144.
- (48) Segota, S.; Heimer, S.; Tezak, D. *Coll. Surf. A* **2006**, *280*, 245–245.
- (49) Segota, S.; Tezak, D.; Talmon, Y. *Soft Materials* **2005**, *3*, 51–69.
- (50) See movie 1movie 2, which show the change in birefringence and the appearance of Maltese crosses upon the L_3-L_α transition.
- (51) Porte, G.; Marignan, J.; Bassereau, P.; May, R. *J. Phys. (Paris)* **1988**, *49*, 511–519.
- (52) Gomati, R.; Appell, J.; Bassereau, P.; Marignan, J.; Porte, G. *J. Phys. Chem.* **1987**, *91*, 6203–6210.
- (53) Marignan, J.; Gauthier-Fournier, F.; Appell, J.; Akoum, F. *J. Phys. Chem.* **1988**, *92*, 440–445.
- (54) Porcar, L.; Hamilton, W. A.; Butler, P. D.; Warr, G. G. *Phys. Rev. Lett.* **2004**, *93*, 198301.
- (55) Hyde, S. *The Language of Shape: The Role of Curvature in Condensed Matter—Physics, Chemistry, and Biology*; Elsevier: Amsterdam Netherlands; New York, 1997.
- (56) Macosko, C. W. *Rheology: Principles, Measurements, and Applications*; VCH: New York, NY, 1993.
- (57) Winter, H. H.; Chambon, F. *J. Rheol.* **1986**, *30*, 367–82.
- (58) Manca, S.; Lapasin, R.; Partal, P.; Gallegos, C. *Rheol. Acta* **2001**, *40*, 128–134.
- (59) Montalvo, G.; Khan, A. *Colloid Polym. Sci.* **2005**, *283*, 402–412.
- (60) Teubner, M.; Strey, R. *J. Chem. Phys.* **1987**, *87*, 3195–3200.
- (61) Schubert, K. V.; Strey, R.; Kline, S. R.; Kaler, E. W. *J. Chem. Phys.* **1994**, *101*, 5343–5355.
- (62) McGrath, K. M. *Langmuir* **1997**, *13*, 1987–1995.
- (63) Strey, R.; Schomacker, R.; Roux, D.; Nallet, F.; Olsson, U. *J. Chem. Soc., Faraday Transactions* **1990**, *86*, 2253–2261.
- (64) Weingärtner, H.; Knocke, A.; Schrader, W.; Kaatze, U. *J. Phys. Chem. A* **2001**, *105*, 8646–8650.
- (65) Hoffmann, H.; Munkert, U.; Thunig, C.; Valiente, M. *J. Colloid Interface Sci.* **1994**, *163*, 217–228.
- (66) Alibert, I.; Coulon, C.; Bellocq, A. M.; Gulik-Krzywicki, T. *Europhys. Lett.* **1997**, *39*, 563–568.
- (67) Mizuno, D.; Nishino, T.; Kimura, Y.; Hayakawa, R. *Phys. Rev. E* **2003**, *67*, 061505.
- (68) Maldonado, A.; Ober, R.; Gulik-Krzywicki, T.; Urbach, W.; Langevin, D. *J. Colloid Interface Sci.* **2007**, *308*, 485–490.
- (69) Vila, J.; Gines, P.; Pico, J. M.; Franjo, C.; Jimenez, E.; Varela, L. M.; Cabeza, O. *Fluid Phase Equilib.* **2006**, *242*, 141–146.
- (70) Vila, J.; Varela, L. M.; Cabeza, O. *Electrochim. Acta* **2007**, *S2*, 7413–7417.
- (71) Tomida, D.; Kumagai, A.; Kenmochi, S.; Qiao, K.; Yokoyama, C. *J. Chem. Eng. Data* **2007**, *S2*, 577–579.
- (72) Harris, K. R.; Kanakubo, M.; Woolf, L. A. *J. Chem. Eng. Data* **2007**, *S2*, 2425–2430.
- (73) Widgren, J. A.; Magee, J. W. *J. Chem. Eng. Data* **2007**, *S2*, 2331–2338.
- (74) Restolho, J.; Serro, A. P.; Mata, J. L.; Saramago, B. *J. Chem. Eng. Data* **2009**, *S4*, 950–955.
- (75) Stoppa, A.; Zech, O.; Kunz, W.; Buchner, R. *J. Chem. Eng. Data* **2010**, *S5*, 1768–1773.
- (76) Sescousse, R.; Le, K. A.; Ries, M. E.; Budtova, T. *J. Phys. Chem. B* **2010**, *114*, 7222–7228.
- (77) Zhang, S.; Lee, K. H.; Frisbie, C. D.; Lodge, T. P. *Macromolecules* **2011**, *44*, 940–949.
- (78) Eiden, P.; Bulut, S.; Köchner, T.; Friedrich, C.; Schubert, T.; Krossing, I. *J. Phys. Chem. B* **2011**, *115*, 300–309.
- (79) Appetecchi, G. B.; Montanino, M.; Carewska, M.; Moreno, M.; Alessandrini, F.; Passerini, S. *Electrochim. Acta* **2011**, *S6*, 1300–1307.
- (80) Vogel, H. *Phys. Z.* **1921**, *22*, 645–646.
- (81) Tamman, G. *Z. Anorg. Allg. Chem.* **1926**, *156*, 245.
- (82) Fulcher, G. S. *J. Am. Ceram. Soc.* **1925**, *8*, 339–355.
- (83) Hiemenz, P. C.; Lodge, T. *Polymer Chemistry*; CRC Press: Boca Raton, FL, 2007.
- (84) Belferres, J. P.; Angell, C. A. *J. Phys. Chem. B* **2007**, *111*, 4926–4937.
- (85) Moynihan, C. T. In *Ionic interactions: from dilute solutions to fused salts*; Petrucci, S., Ed.; Academic Press: New York, 1971; Vol. 1; p 262.
- (86) Shanks, P. C.; Franses, E. I. *J. Phys. Chem.* **1992**, *96*, 1794–1805.
- (87) Soubiran, L.; Coulon, C.; Sierro, P.; Roux, D. *Europhys. Lett.* **1995**, *31*, 243–248.
- (88) Roux, D.; Coulon, C.; Cates, M. E. *J. Phys. Chem.* **1992**, *96*, 4174–4187.